DOI 10.1515/aot-2013-0023 — Adv. Opt. Techn. 2014; 3(1): 41–53

Tutorial

Olaf Stenzel*

The impact of the mass density on selected optical and non-optical properties of oxide coatings

Abstract: The density of optical coatings is one of the most crucial material-related parameters in interference coating science and technology. It has an impact on the refractive index, the transparency range, and the mechanical stress of a coating material. This tutorial provides a background on the classical theory relating the coating density to the mentioned parameters. Simple models are presented that highlight the correlations between optical constants, stress, and shifting behavior of different oxide coatings. Comparison with the experiment is performed on the basis of numerous experimental data, which stem from hafnium oxide, zirconium oxide, tantalum pentoxide, and silicon dioxide.

Keywords: absorption edge; density; mechanical stress; oxide coatings; refractive index; shift.

OCIS codes: 310.6860; 310.6870; 310.1620.

***Corresponding author: Olaf Stenzel,** Fraunhofer IOF Jena, Albert-Einstein-Str. 7, 07745 Jena, Germany, e-mail: Olaf.stenzel@iof.fraunhofer.de

1 Introduction

Any optical phenomenon is in some way connected to the interaction of electromagnetic radiation with matter. This interaction may be theoretically treated at different conceptual levels. For example, there are many cases where a purely classical description may find an application. It is, on the other hand, possible to build a strong quantum mechanical theory. A purely classical description makes use of Maxwell's equations for the description of the electrical and magnetic fields and classical models (for example, Newton's equations of motion) for the dynamics of the charge carriers present in any terrestrial matter. On the contrary, a quantum mechanical treatment is performed within the framework of the quantization of the electromagnetic field (so-called second quantization) and a quantum theoretical treatment of matter. This description is necessary, when spontaneous optical effects have to be described (spontaneous emission, spontaneous Raman scattering, or spontaneous paramagnetic interactions in nonlinear optics). In applied spectroscopy, the accurate quantum mechanical description is often omitted due to the rather complicated mathematics and replaced by the so-called semiclassical treatment. Here, the properties of matter are described in terms of quantum mechanical models, while the electromagnetic fields are treated within the framework of Maxwell's theory.

In practice, a large number of practically important problems may be solved working with classical models only. It is the purpose of this tutorial to give an introduction into the physics behind major practically relevant correlations between optical and mechanical film properties, mainly in the language of classical physics.

The focus of this tutorial is on optical material parameters like refractive index n, extinction coefficient k, absorption edge (optical gap=photon energy corresponding to the absorption onset) E_{gap}, thermal or vacuum shift, and mechanical stress σ of dielectric coating materials. All these parameters are highly relevant in any feasible design and practical application of optical coatings. Here, at least the optical parameters definitely describe certain facets of the earlier mentioned rather general problem of interaction of light with matter, and it is intuitively clear that this interaction will be more efficient and pronounced when the amount of matter in the considered volume element in increased. Therefore, at any of the mentioned levels for describing the light-with-matter interaction of macroscopic systems, parameters like concentration, particle density, or mass density play a crucial role.

This turns us, in a rather natural manner, to the main topic of this tutorial. Here we will discuss handable classical models for estimating the effects of density and porosity on the mentioned material parameters, primarily with respect to oxide coatings. For the outset we should

say that the discussion of effects of crystallinity, stoichiometry, and contaminations is outside of the scope of this tutorial.

2 Dispersion of optical constants

The optical constants n and k of an optically homogeneous and isotropic nonmagnetic optical material are directly related to its complex dielectric function $\varepsilon(\omega)$ through the relationship:

$$n+ik=\sqrt{\varepsilon(\omega)}=n(\omega)+ik(\omega)=\hat{n}(\omega) \tag{1}$$

In Eq. (1), ω is the angular frequency of the incident light wave, and $\hat{n}(\omega)$ is called the *complex index of refraction*. Hereby, the ω-dependence of the dielectric function and the optical constants is called *dispersion*. The concrete type of frequency dependence is expressed in terms of the relevant *dispersion model*.

The simplest classical model to describe the optical properties of an insulator is the so-called single oscillator model. It is relevant for describing the optical behavior of the bound charge carriers in a solid. Let us assume the solid to be built up from rather microscopic units (atoms, molecules) with a concentration N. Under the action of Coulombs force as caused by the local electric field of the light wave E_{micr}, each of the microscopic charge carriers performs forced oscillations, which result in an oscillating microscopic dipole moment p. Let us introduce the microscopic polarizability β according to the definition (SI units):

$$p\equiv\varepsilon_0\beta E_{micr} \tag{2}$$

In terms of a mass-on-a-spring model, the interaction of visible or UV light with the atoms of matter appears to mainly result in oscillations of the light electrons (with mass m and charge q) relative to the heavy (and, therefore, rather immobile) atomic cores (Figure 1, left). This idea leads us to the following expression for the complex microscopic polarizability [1]:

$$\beta=\beta(\omega)=\frac{q^2}{\varepsilon_0 m}\frac{1}{\omega_0^2-\omega^2-2i\omega\gamma} \tag{3}$$

In Eq. (3), ω_0 is the resonance angular frequency of a selected microscopic oscillator. Eq. (3) gives rise to the dispersion behavior of optical constants specific to what is called the Lorentzian oscillator model.

The relation between the microscopic polarizability and the macroscopic optical constants is obtained when explicitly distinguishing between microscopic (local) and macroscopic (average) electric fields of the light wave. The, perhaps, most accessible approach to this complex of problems is given in [2]. It turns out that the complex index of refraction is a complicated function of the polarizability and density of the assumed microscopic units, as well as on their shape. The latter may be quantified in terms of a depolarization factor L [3, 4]. In the most compact terms, this dependence can be expressed in terms of Eq. (4):

$$\frac{\hat{n}^2-1}{\hat{n}^2L+(1-L)}=N\beta \tag{4}$$

In optically isotropic materials, spherical symmetry of the microscopic units building the solid is usually assumed, corresponding to L=1/3. Then, from Eq. (4), the typical writing of the Lorentz-Lorenz formula is obtained:

$$\frac{\hat{n}^2-1}{\hat{n}^2+2}=\frac{N\beta}{3} \tag{5}$$

The good news is that equations like Eqs. (4) and (5) give direct access to the classical dependence of the optical constants on film density ρ. Indeed, as soon as the concentration of microscopic dipoles is assumed to be proportional to the mass density, from Eq. (4), we find immediately:

$$\hat{n}^2=\hat{n}^2(\omega)=1+\frac{\frac{Nq^2}{\varepsilon_0 m}}{\left[\omega_0^2-L\frac{Nq^2}{\varepsilon_0 m}\right]-\omega^2-2i\omega\gamma};\ N\propto\rho \tag{6}$$

Let us analyze this equation in more detail. Obviously, Eq. (6) describes resonance behavior when the angular frequency of the light comes close to a resonance frequency given in brackets in Eq. (6) (see Figure 1, right).

For electronic polarization, in many materials, this frequency corresponds to the UV spectral region. This

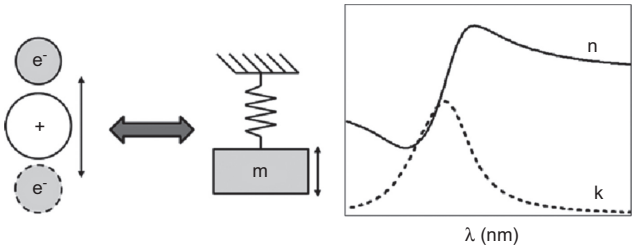

Figure 1 Left: classical idea of an oscillating dipole moment formed by the motion of an electron relative to the heavy atomic core, and oscillating mass on a spring as the mechanical analogue; right: corresponding dispersion of optical constants as described by Eq. (6) in the vicinity of the resonance. The wavelength scale is reciprocally stretched to preserve symmetry.

allows us distinguishing between three main spectral regions. Their specifics are explained in Table 1.

3 Optical constants and mass density

3.1 Refractive index

In interference coating science and technology, in the majority of cases, we work in the first of the spectral regions introduced in Table 1, and we will further focus on it. So we assume that the light frequency is small enough in order to avoid absorption due to resonant excitation of valence electrons in the material, while the onset of the latter is defining the fundamental absorption edge. In this first spectral region, materials are almost transparent, while according to Eq. (6), an increase in density should be clearly accompanied by an increase in the refractive index. This is visualized in Figure 2, top left.

Left on top in Figure 2, we recognize the expected trend of increasing refractive index with increasing density. In the other fields of the figure, corresponding experimental data are collected, which stem from various oxide materials (HfO_2 [5, 6], Ta_2O_5 [7], ZrO_2 [6]), which are obviously consistent with the theoretical prediction. The differences in mass density of these coatings have been achieved by varying certain corresponding process parameters in the course of either electron beam evaporation (EBE) or plasma ion-assisted deposition (PIAD). A description of the PIAD method is given in [8].

3.2 Absorption onset

Let us now turn to the absorption behavior. The classical Eq. (6) cannot, of course, describe a phenomenon like the formation of an absorption edge in a solid material in a quantitatively correct manner. Rather the resonance in Eq. (6) describes the central frequency of an absorption band, while the onset frequency of the absorption structure (fundamental absorption edge or simply optical gap) is connected to the flank of that absorption feature. Hence, the absorption behavior at the high-frequency edge of spectral region 1 will qualitatively look similar to what is shown in Figure 3. It is, nevertheless, reasonable to assume, that a red shift in the central frequency of the absorption feature is accompanied with a red shift of the absorption onset frequency. As it results from the second column in Table 1, an increase in the film density tends to narrow the spectral region 1, a phenomenon that we can qualitatively assign with the shift of the absorption onset frequency. Hence, as long as we speak about interference coatings working in the first spectral region from Table 1, an increase in density is expected to result in a higher refractive index but, at the same time, in a shift of the absorption onset to lower frequencies.

Table 1 Classification of spectral regions with respect to the resonance frequency.

Spectral region	Criterion	*n*, *k*	Application
1	$\omega^2 << \left[\omega_0^2 - L\frac{Nq^2}{\varepsilon_0 m}\right]$	$n^2 \approx 1 + \frac{\frac{Nq^2}{\varepsilon_0 m}}{\left[\omega_0^2 - L\frac{Nq^2}{\varepsilon_0 m}\right] - \omega^2} > 1$ (Normal dispersion) $k << n$	IR/VIS/UV interference coating
2	$\omega^2 \approx \left[\omega_0^2 - L\frac{Nq^2}{\varepsilon_0 m}\right]$	According to Eq. (6); strong anomalous dispersion $k \sim n$	(UV) absorber
3	$\omega^2 >> \left[\omega_0^2 - L\frac{Nq^2}{\varepsilon_0 m}\right]$	$n^2 \approx 1 - \frac{Nq^2}{\varepsilon_0 m\omega^2} < 1$ (Normal dispersion) $k \approx (1-n^2)\frac{\gamma}{\omega} << n$	EUV/X-ray interference coating

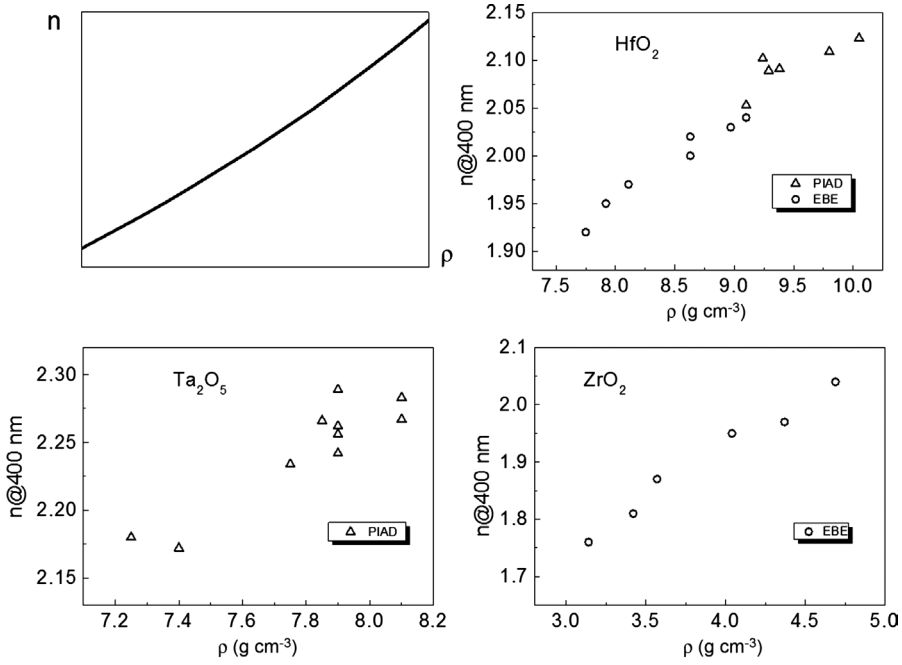

Figure 2 Left on top: relation between refractive index and mass density as predicted by Eq. (6); right on top: experimental data for hafnium oxide films; left on bottom: experimental data for tantalum pentoxide; right on bottom: experimental data for zirconium oxide.

When comparing this prediction with experimental data, the question on how to determine the optical gap in practice is naturally raised. There are two basic groups of methods for quantifying the optical gap in practice. One method is entirely based on the evaluation of so-called Tauc plots or Cody plots [9]. Practically, that means that a certain model behavior of the absorption coefficient, which has proven to fit the experimental data in a certain spectral range, is to be extrapolated to zero absorption. The corresponding photon energy marks the value of the optical (Tauc or Cody) gap (see Figure 3).

The second method is more pragmatic. Once the absorption coefficient has been determined and found to be similar in shape to that shown in Figure 3, the gap is determined as the photon energy where the absorption coefficient reaches a certain threshold value. Thus, the so-called E_{04} gap ([10]) corresponds to the photon energy, where the absorption coefficient is equal to 10^4 cm^{-1}. As seen in Figure 3, the E_{04} gap is expected to be different from the Tauc gap. However, in the case where the absorption edge is very steep, both values may be rather close to each other. In this tutorial, for the sake of simplicity, we will characterize the absorption onset in terms of the E_{04} gap (Figure 4).

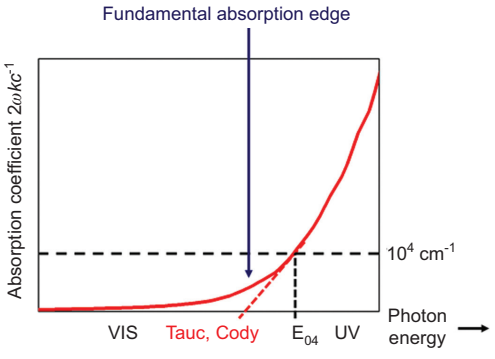

Figure 3 Absorption coefficient in the region of the absorption edge and illustration of different optical gap definitions. *c*, speed of light in vacuum.

In Figure 4, we again recognize a principal similarity between the theoretical prediction from Eq. (6) and the general trend following from the experimental data. The degree of accordance is clearly not as good as in Figure 2 for at least two reasons. First, Eq. (6) predicts the behavior of a single resonance frequency only, while the experimental observable (E_{04} gap) is only a very rough analog to that frequency. Second, we should take into account, here, that the sensitivity of the E_{04} gap to possible contaminations and stoichiometry effects, which are not taken into account in our simple calculations, will be considerably higher than that of the refractive index.

But all in all, both the simple classical oscillator model as well as the presented experimental data confirm to us the important trend of an increasing refractive index with increasing film density. At the same time, the absorption edge shows a trend to shift

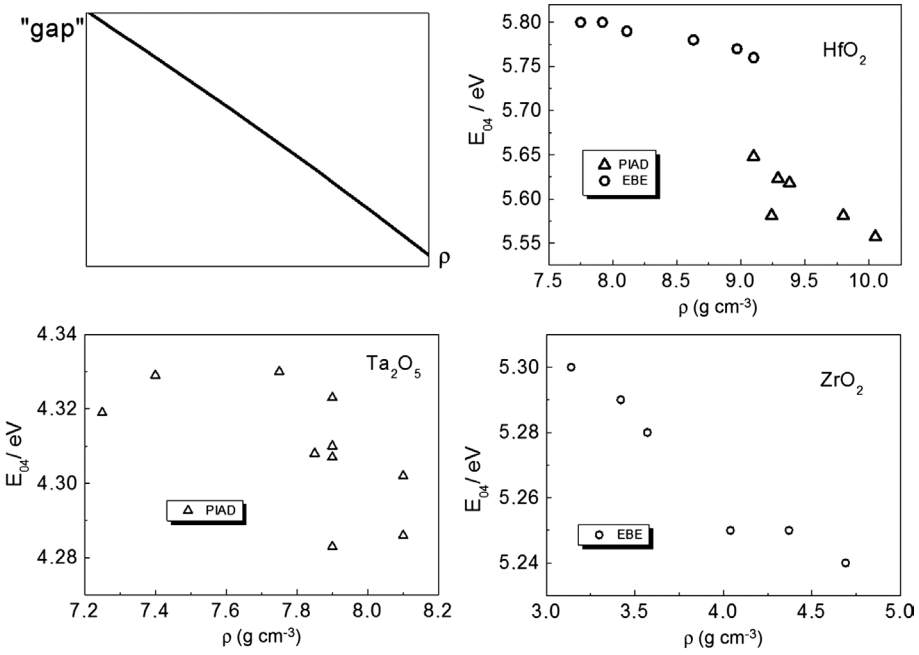

Figure 4 Top left: relation between the absorption edge position ('gap') and mass density as predicted by Eq. (6); top right: experimental data for hafnium oxide films [5, 6]; bottom left: experimental data for tantalum pentoxide [7]; bottom right: experimental data for zirconium oxide [6].

toward a longer wavelength (or lower photon energies). These are simple facts that we have to accept. It is worth mentioning that the same trends are observed in terms of strong quantum mechanical calculations. Thus, in the reference [11], quantum mechanical calculations of the dielectric function of amorphous and crystalline titanium dioxide materials also lead to a decrease in the optical gap (in that study, the Tauc gap) and an increase in refractive index when the assumed film density is increased. This trend is observed for amorphous as well as crystalline phases. So that, although oxide coatings are often amorphous when being deposited by plasma- or ion-assisted techniques, a certain crystalline fraction does not necessarily violate the predicted trends. However, the coatings prepared by electron beam evaporation without assistance are usually polycrystalline. They show essentially the same behavior when the (average) density is changed, but the corresponding data may appear to be aligned in a somewhat different manner as the assisted samples, as seen, for example, in Figure 4, top right.

The mentioned trends observed in all the examples highlight the role of the film density as a key parameter responsible for the actual values of the optical constants. But the effect of the density is, in fact, relevant even for a broader spectrum of film properties.

4 Mass density and mechanical stress: a naïve model

The key role of the mass density for a broad complex of coating properties becomes especially clear when looking in more detail at the atomic structure of the discussed thin film material. At low temperatures, the atomic cores in a solid may be imagined to be practically at rest at a position localized in the minimum of some potential curve, which describes the interatomic potential. In order to highlight the main effects, let us restrict on a very simplified model case, where the interaction between all the atoms with their neighbors is described by the same potential curve. Hence, in this 'naïve model', we focus on our discussion to a pair of atoms only. The corresponding interatomic potential U will look similar to what is shown in Figure 5.

At the abscissa in Figure 5, we see the interatomic distance, which we will identify with the symbol r. The potential has a local minimum at some equilibrium distance r_0, which corresponds to some equilibrium distance between the atoms. Any deviation from this distance gives rise to a higher potential energy and, therefore, to a restoring force, which drives the atoms back to their equilibrium position. The restoring force is given by:

$$F=-\nabla U \tag{7}$$

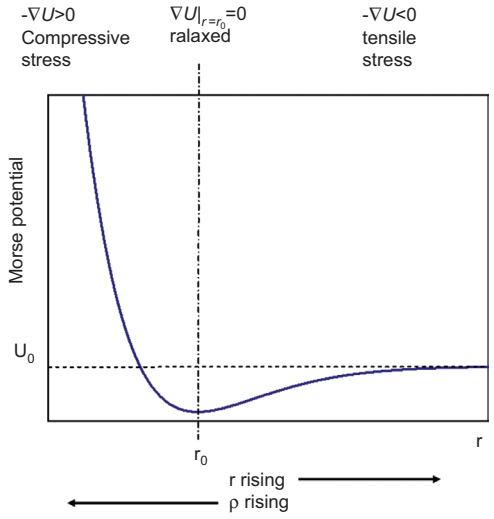

Figure 5 Assumed shape of the interatomic potential as a function of the interatomic spacing.

At r_0, the gradient in Eq. (7) is zero, and therefore, the atoms do not experience any elastic force, which would drive them to another position. Therefore, that distance r_0 marks some interatomic distance where the solid is mechanically relaxed. Moreover, this interatomic distance corresponds to a certain mass density ρ_0. Keeping in mind our previous discussion, this mechanically relaxed state must also correspond to a certain refractive index $n_0=n(\rho_0)$. Let us take this relaxed state as the starting point for our further discussion.

As previously discussed, the refractive index may be enhanced by increasing the film density. But this must be accompanied by a decrease in the interatomic distance. According to Eq. (7) and Figure 5, a decrease in r will result in a force acting on every atom, which drives the solid to re-expand its volume (F>0), so that the solid with the higher density is no more mechanically relaxed, but suffers some internal stress, which we call a compressive stess. Obviously, that stress will become stronger when the density is further increased, or the interatomic distance is decreased. Therefore, the enhancement of the refractive index through densification of the material should result in the appearance of compressive stress.

Let us now consider the opposite case. A decrease in density is accompanied by an increase in r. Again, that will give rise to an elastic force, which is now directed in the opposite direction (F<0): it now tends to re-tighten the solid. This is what we call a tensile stress. It behaves differently from the compressive stress in the sense that a further decrease in density will first result in an increase of the absolute value of the tensile stress, but after having passed a turning point in the potential curve in Figure 5, the stress will relax and converge to zero when the density approaches zero (infinitely large interatomic distance). This is understandable because, in this case, we no longer have any solid material, but only isolated atoms, which do no more than interact with each other.

This simplest model discussion leads us to a very important result: when affecting the film refractive index through changes in the film density, we will necessarily affect the film stress as well. Practically, that means that the refractive index and stress are expected to show some correlation. This is an extremely important conclusion because it follows that it does not make sense to specify optical and mechanical properties of a coating material independently from each other. Let us look at how far such correlations are really observed.

In Figure 6, experimental refractive index data of selected oxide materials are opposed to the measured mechanical stress. In accordance with our previous discussion, positive stress values correspond here to compressive stress, while negative values correspond to tensile stress. Please note that in other sources, the opposite convention may be used. The interesting point is that the experimental data points are indeed not statistically distributed, but are arranged more or less closely to some knee-like dependence, which seems to look similar for all these different materials. This is all the more interesting, as the data collected in Figure 6 stem from even more diverse coating deposition techniques, including the now ion-assisted deposition (IAD) ion plating (IP), magnetron sputtering (MS), plasma-enhanced reactive magnetron sputtering (PARMS), and ion beam sputtering (IBS). The data are collected from the following sources [5–7, 12–15].

From Figure 6, we recognize another typical trend. From the arrangement of data, we learn that unassisted electron beam-evaporated samples tend to have lowest densities, lowest refractive indices and low or moderate tensile mechanical stress. Highest refractive indices (and densities) as well as the strongest compressive stress is typical for IP-deposited samples. (P)IAD and sputtering techniques tend to fall in between the extreme cases mentioned.

Let us now use our simple model to get a mathematical expression that describes the major trend in the arrangement of experimental points from Figure 6. First, we have to postulate a mathematical expression for the potential curve given in Figure 5. A Lennard Jones potential or the Morse potential are good candidates. We will use the Morse potential [16]:

$$U=U_0\left(1\text{-}e^{-\frac{r\text{-}r_0}{a}}\right)^2 \tag{8}$$

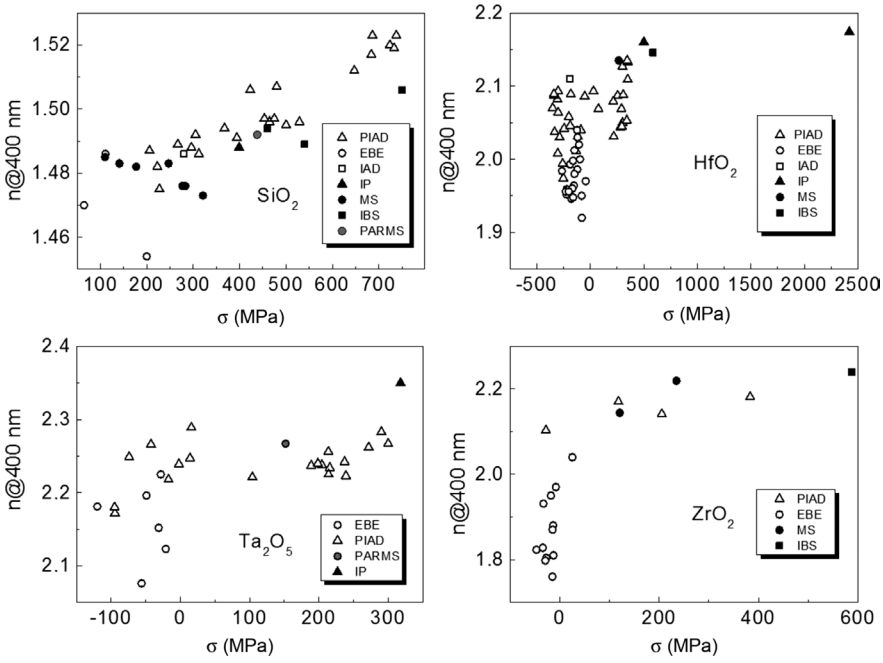

Figure 6 Relation between refractive index and mechanical stress; top left: experimental data for silicon dioxide films [7, 12–14]; top right: experimental data for hafnium oxide films [5–7, 12, 15]; bottom left: experimental data for tantalum pentoxide [7, 12–14]; bottom right: experimental data for zirconium oxide [6, 15].

with a as some further constant. From here, we immediately find an expression for the elastic force F acting between the atoms:

$$F=-\frac{dU}{dr}=-\frac{2U_0}{a}\left(1-e^{-\frac{r-r_0}{a}}\right)e^{-\frac{r-r_0}{a}} \tag{9}$$

which is zero for $r=r_0$. Hence, it makes sense to model the stress σ via the expression:

$$\sigma(r)=-const.\left(1-e^{-\frac{r-r_0}{a}}\right)e^{-\frac{r-r_0}{a}} \tag{10}$$

Here, $const.>0$ holds according to Eq. (9). This kind of dependence is visualized in Figure 7.

The stress is zero for $r=r_0$, which corresponds to a certain film density ρ_0. Here, we have:

$$r\propto\sqrt[3]{\frac{1}{\rho}};\ r_0\propto\sqrt[3]{\frac{1}{\rho_0}} \tag{11}$$

The relations (10) and (11) are sufficient to predict a dependence of the mechanical stress on the interatomic distance as well as on the density in terms of the Morse potential. This is visualized in Figure 7.

The striking feature in Figure 7 on the bottom is that the tensile stress does not exceed a certain extremal value $-\sigma_{\text{tensile, max}}$. Let us express this value through the parameters entering into Eq. (10). Differentiating Eq. (10) with respect to r results in:

$$\frac{d\sigma}{dr}=-\frac{const.}{a}\left(2e^{-2\frac{r-r_0}{a}}-e^{-\frac{r-r_0}{a}}\right) \tag{12}$$

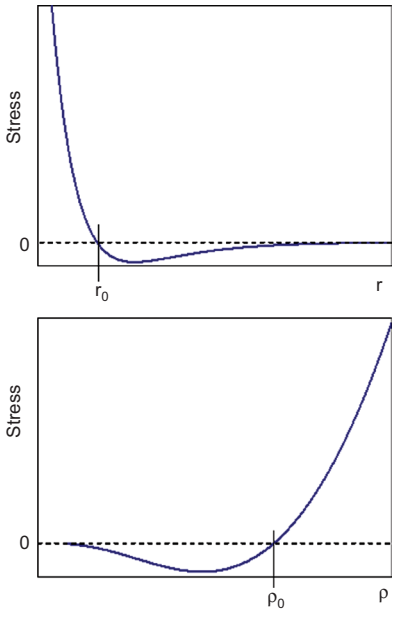

Figure 7 Dependence of the stress on interatomic distance and mass density following Eqs. (10) and (11).

This derivative must be zero when the stress equals $\sigma_{\text{tensile, max}}$. As it follows from Eq. (12), this is observed at:

$$r=r_0+a\ln 2 \tag{13}$$

Then, from Eq. (12), we obtain:

$$\sigma_{\text{tensile, max}}=\text{-}const.\left(1\text{-}e^{-\frac{r-r_0}{a}}\right)e^{-\frac{r-r_0}{a}}\Bigg|_{r=r_0+a\ln 2}=\frac{\text{-}const.}{4} \tag{14}$$

or

$$\sigma=4\sigma_{\text{tensile, max}}\left(1\text{-}e^{-\frac{r-r_0}{a}}\right)e^{-\frac{r-r_0}{a}} \tag{15}$$

The parameter $\sigma_{\text{tensile,max}}$ is easily estimated from experimental data like those shown in Figure 6. It substitutes the less accessible parameter U_0.

According to Eq. (4), we can further write:

$$\begin{aligned}\rho\propto r^{-3}\propto\frac{n^2\text{-}1}{n^2+2}\\ \rho_0\propto r_0^{-3}\propto\frac{n_0^2\text{-}1}{n_0^2+2}\end{aligned} \tag{16}$$

This allows us to substitute the values r and r_0 from Eq. (15) by the corresponding refractive indices. We obtain the final result:

$$\sigma(n)=4\sigma_{\text{tensile, max}}\left(1\text{-}e^{-b\left[\sqrt[3]{\frac{n^2+2}{n^2\text{-}1}}-\sqrt[3]{\frac{n_0^2+2}{n_0^2\text{-}1}}\right]}\right)e^{-b\left[\sqrt[3]{\frac{n^2+2}{n^2\text{-}1}}-\sqrt[3]{\frac{n_0^2+2}{n_0^2\text{-}1}}\right]} \tag{17}$$

Here, a dependence between stress and refractive index following from an assumed Morse potential is explicitly formulated. There is one remaining free parameter b, which combines information about the Morse parameter a and the proportionality constants in Eq. (16). It may be tackled as a fitting parameter.

As an example, let us look at Figure 8 on the left. It shows the experimental data on the correlation between stress and refractive index for the special case of tantala layers (data taken from Figure 6). From the experimental data, one may easily estimate $\sigma_{\text{tensile,max}}$ ≈-140 MPa, and n_0≈2.25. Although our model assumptions are rather simple, we recognize a rather good correspondence between the calculated, by Eq. (17), theoretical dependence (full line) and the major trend in the arrangement of data points even in the region of tensile stress. This has been achieved by a proper choice of the dimensionless parameter b, which had been set to b=70 in this calculation. In fact, it is that additional parameter that allows us to obtain *ad hoc* theoretical graphs for describing the relation between stress and refractive index in a material that is structurally much more complicated than the assumed homogeneous assembly of Morse oscillators. A corresponding calculation assuming b=13 is shown in Figure 8, right, for the zirconia coatings.

We notice the small ascent of the n=$n(\sigma)$ dependence at high compressive stress. This offers certain potential for compressive stress relaxation without significant impact on the refractive index, as achieved by means of thermal annealing of highly densified oxide coatings.

5 Closer to reality: effects of pores

5.1 Visualization of pores in a coating

Of course, what we have discussed, so far, is a rather idealized model. In practice, one will never observe such homogeneous increase in interatomic spacings when the average density of a coating is decreased. On the contrary, low-density coatings tend to be porous, i.e., show severe fluctuations in local density. These pores may be visualized by means of transmission electron microscopy. Some examples of porous PIAD coatings are given in Figure 9. In the examples shown, elongated pores appear as the result of what we call a columnar film growth. The

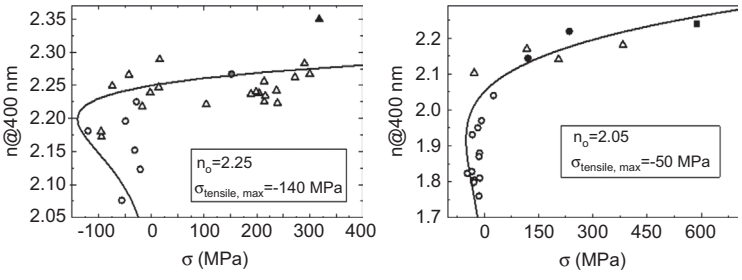

Figure 8 Refractive index vs. mechanical stress for tantala coatings (left, symbols as in Figure 6), and zirconia coatings (right). The full line shows the theoretical dependence according to Eq. (17).

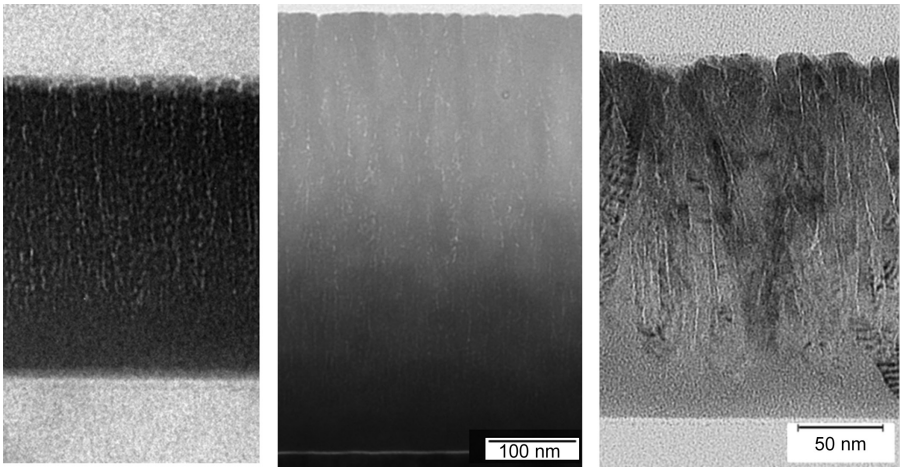

Figure 9 Cross-sectional transmission electron microscopy images of porous niobia (left), tantala (center), and hafnia (right) coatings. The pores appear as thin, bright, elongated structures.

images in Figure 9 reveal an important secondary effect of the columnar growth: When the pores open to the film surface, they give rise to a certain so-called small-scale surface roughness of the coating.

Once pores tend to decrease the refractive index and to induce tensile stress, the appearance of pores principally leads to a qualitatively similar dependence of the refractive index and the stress on the mass density, as it has been shown earlier in Figures 2 and 6. Therefore, a similar correlation between refractive index and stress like those presented in Figures 6 and 8 will be obtained, as it has been shown by corresponding model calculations [17]. The additional assumption of the existence of a pore fraction does, therefore, not seriously violate our calculations performed so far, but the pores give rise to a further phenomenon, which is called the shift of the coating.

5.2 Shift behavior

The point is that porous coatings are likely to show a relevant thermal and vacuum shift because water can penetrate into the pores when the coating is exposed to air at room temperature. Clearly, the refractive index of a system, which is composed from a solid fraction and pores, will depend on whether the pores are empty or filled with water. Here, the *thermal shift* is defined as the relative change in optical thickness of the coating caused by a change in temperature. In many cases, the measurement of the thermal shift is performed by heating the samples in atmospheric conditions. The *vacuum shift* denotes the corresponding change in optical thickness, when the coating is brought from vacuum into air, keeping the temperature constant. In the case of porous layers, the observed change in optical thickness is usually dominated by changes in the refractive index, which in turn is caused by changes in the water content in the pores when the sample is evacuated or/and heated. Thus, the shift can be defined through:

$$shift = \frac{\Delta(nd)}{nd} \times 100\% = \frac{\Delta n}{n} \times 100\% + \frac{\Delta d}{d} \times 100\% \qquad (18)$$

It is, therefore, possible to get an impression on the porosity of a sample measuring a superposition of the thermal and vacuum shift. This should not be done immediately after deposition, but rather at least after several days of film exposure to the atmosphere, so that at least, the large pores in the films can be expected to be filled with water. First, a transmission measurement is performed in atmospheric conditions at room temperature. After that, the measurement chamber has to be evacuated to high vacuum and heated up to a temperature of 100°C before making the second transmission measurement. In these conditions, the pores are expected to be free of water. That leads to a change in optical thickness and, correspondingly, to a wavelength shift of the interference extrema in the transmission or reflection spectrum of the film. Then, the shift can be determined from the wavelength shift of a selected interference extremum λ_m by:

$$shift = \frac{\lambda_{m,\,100°C} - \lambda_{m,\,room\ temperature}}{\lambda_{m,\,room\ temperature}} \times 100\% \qquad (19)$$

All in all, low-density coatings, which usually appear to be porous, shall show a much stronger shifting behavior than dense (pore-free) coatings. Therefore, the refractive

index, stress, and shift shall be strongly correlated within the frames of a given coating material.

5.3 Correlation between shift and mechanical stress

We will not present here a full derivation of that correlation explicitly taking porosity into account. The reader is kindly referred to [17], where a corresponding calculation is performed. We will restrict ourselves here to a rather qualitative illustration. Let us state here instead, that there is numerous empirical material accumulated, which verifies that strongly porous coatings tend to exhibit tensile stress. It is well proven that dense, pore-free coatings tend to exhibit significant compressive stress. On the other hand, once the porosity comes close to 100%, the stress should be zero because there is no longer any solid. Assuming at the same time that the dependence of the stress on the porosity should be a mathematically continuous function, we find that the behavior of the stress as a function of porosity cannot be a monotonous function. This principal behavior is illustrated in Figure 10 (top).

First of all, Figure 10 reflects the mentioned rule that remarkable compressive stress is observed whenever the porosity is low. An increase in porosity is then accompanied by a decrease in stress, until the latter changes to tensile stress. This means that the stress must be zero at a certain, rather low, porosity level. A further increase in porosity results in tensile stress. Nevertheless, at highest porosity, the stress must again converge to zero. From here, it follows that the curve must show at least one extremum, which corresponds to a local minimum in stress or a local maximum in tensile stress, in complete accordance to our earlier discussion in Section 4.

Therefore, we have to expect *two* regions of porosity, where the mechanical stress is low by absolute value or ideally zero. We expect low stress at highest porosity levels, but this regime is not very interesting from the practical point of view. There is also a regime of rather low porosity where stress is negligible, when a low number of possibly very small pores compensate the compressive intrinsic stress of the solid atomic network. This regime is of the highest practical interest. The reason is that because of the still low porosity, the shift (Figure 10, center) is expected to also be very small. On the contrary, the shift is expected to be strongest at high porosity levels. The behavior of the shift, as defined by Eq. (19) as a function of porosity, should, therefore, correspond to what is sketched in Figure 10 (center).

It is, of course, difficult to verify these dependencies on porosity experimentally because it is difficult to measure the porosity directly in a quantitative manner, it is more convenient to establish the thus defined correlation between stress and shift. We will then obtain a knee-shaped dependence as qualitatively shown in Figure 10, bottom. At a certain, rather low, porosity level, this dependence predicts both the mechanical stress and the shift to be negligible. This coincidence of vanishing shift and stress is what we call *balanced coating properties*.

In Figure 11, corresponding experimental data are again collected. Despite the silicon dioxide, which shows remarkable compressive stress even in strongly shifting samples, the data arrange in a manner that resembles

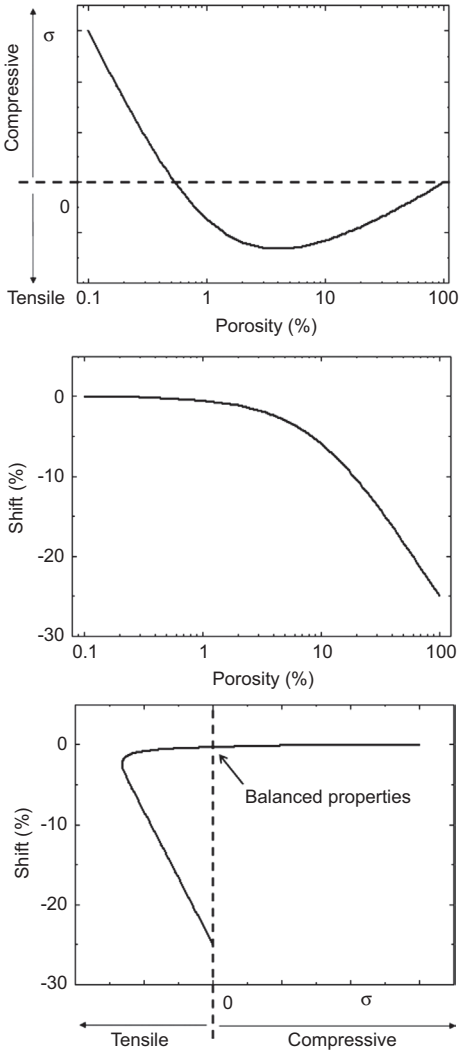

Figure 10 Top: expected behavior of the film stress as a function of porosity; center: expected behavior of the shift as a function of porosity; bottom: expected correlation between the film stress and the shift.

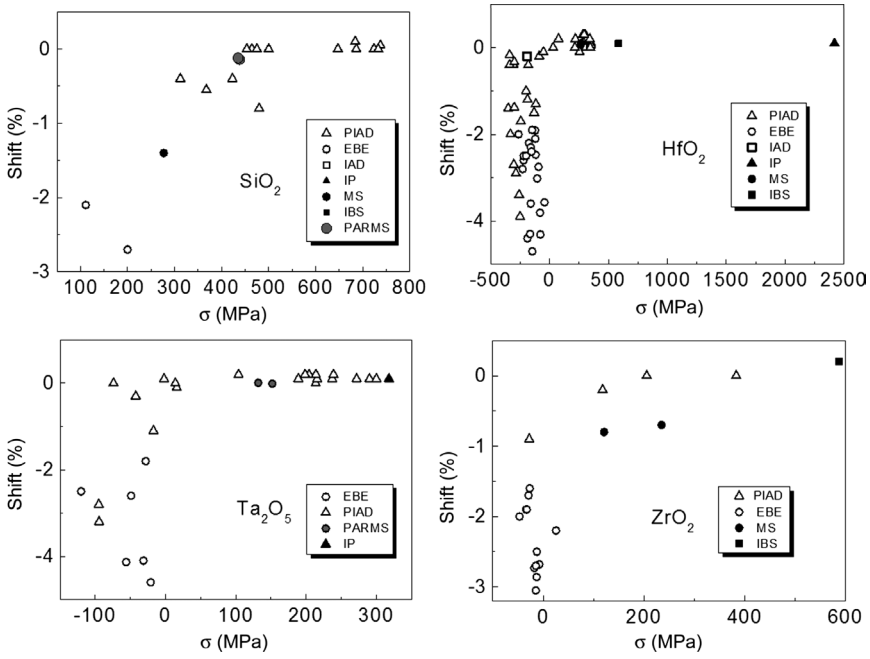

Figure 11 Relation between shift and mechanical stress; top left: experimental data for silicon dioxide films [7, 12–14]; top right: experimental data for hafnium oxide films [5–7, 12, 15]; bottom left: experimental data for tantalum pentoxide [7, 12–14]; bottom right: experimental data for zirconium oxide [6, 15].

the principal shape of the theoretical curve presented in Figure 10 (right). At least, in the cases of tantala and hafnia layers, we identify certain PIAD samples, which show the mentioned balanced coating properties.

While emphasizing once more that this is a tutorial and not a research paper, it is worth mentioning that correlations between optical and mechanical properties are nothing principally new in thin film optics. Thus, it is well-known, that simple relationships between infrared transmission and mechanical properties of IR coatings result from the same type of interatomic potential as shown in Figure 5. Indeed, the steeper the potential curve, the higher is the elastic constant, and the higher the IR Reststrahlen absorption frequencies will be [18]. This made it so difficult to identify the hard and durable coating materials, which are at the same time transparent in the wavelength range between 8 and 12 µm [19].

6 A few remarks on experimental techniques

A collection of experimental data like those presented in this tutorial requires a tremendous amount of experimental film deposition, measurement, and data evaluation effort. It is therefore worth providing information here about the principal experimental techniques, which have found application when creating the experimental database, which has been used in this tutorial. The techniques will be shortly mentioned, together with references for further reading.

When determining the thin-film refractive indices and absorption coefficients, spectrophotometric or spectroellipsometric measurements represent the most frequently applied techniques today. The optical constants and gaps as presented in this study all arise from spectrophotometric measurements and subsequent curve fitting procedures using Kramers-Kronig-consistent dispersion models. Details on this kind of procedure can be found in [20, 21]. For details on the variable angle spectroscopic ellipsometry, the reader is kindly referred to [22].

For shift measurements, we used the *in situ* transmission spectrophotometer OptiMon [23]. More details on the methodology can be found in [12]. The mechanical stress has been determined from strain measurements performed here utilizing Tencor equipment. A comparative study of the different stress determination techniques can be found in the collaborative study [24].

The reported mass density values have been obtained from X-ray-reflection (XRR) measurements at the total reflection onset. The corresponding theoretical background is described in [25]. The visualization of pores by means of cross-sectional transmission electron microscopy

(TEM) is very impressive and gives rather direct evidence on the existence of the pores, but due to the expense and complexity of both the cross-sectional sample preparation technology and the necessary equipment, it is far from being a routine characterization tool in a typical optical coating lab or company today. As outlined in Section 5.3, a 'quick and dirty' judgment on the degree of porosity of larger sample numbers is also possible from a combination of shift and mechanical stress measurements.

7 Summary

Variations in coating density as well as in the degree of porosity, depending on the deposition technique and conditions chosen, have a crucial impact on the optical and mechanical coating properties. Particularly with respect to IAD and PIAD techniques, a change in deposition conditions offers a certain flexibility to achieve tailored values of interesting parameters within certain limits.

With that in mind, the present study was focused on the correlations between parameters like stress, refractive index, absorption onset frequency, and layer stress, as dictated by the underlying dependence on density and porosity. Those correlations are derived theoretically in the framework of classical models and verified by numerous experimental material. The highlighted correlations appear to be valid for different coating materials.

Knowledge of these correlations is important for the consistent choice of coating materials and deposition conditions, in order to match the sophisticated design specifications including optical and non-optical targets. They supply a general frame for reasonable and consistent specifying of optical coatings performance.

Acknowledgments: The author would like to thank Prof. Angus Macleod for the invitation to contribute this tutorial to this special issue of *Advanced Optical Technologies*. It appeared straightforward to give a survey on simple classical models, but as soon as any practically relevant theory is to be supported or falsified by experimental data, it appeared necessary to complete the text with comprehensive experimental material. The latter had been collected over the latest decade by many of my colleagues and collaborators, and it is impossible to mention all of them here. Instead, I would like to express my thanks *en masse* to the consortia of the projects IntIon, nanomorph, TACo, TAILOR, and PluTO, and to acknowledge the support by the sponsoring ministries – the BMWi, the BMWA, and the BMBF in Germany. More concrete data on the collaborators and companies/institutions are found in the author lists and acknowledgments of the cited references. Technical assistance in the figure and manuscript preparation has been provided by Josephine Wolf and Steffen Wilbrandt (both IOF in Jena). The TEM images from Figure 9 was supplied by Prof. Ute Kaiser, Ulm University, Germany.

Received May 16, 2013; accepted May 22, 2013; previously published online July 4, 2013

References

[1] M. Born and E. Wolf, in 'Principles of Optics', (Pergamon Press, Oxford London Edinburgh New York Paris Frankfurt, 1968).
[2] R. P. Feynman, R. B. Leighton and M. Sands, in 'The Feynman Lectures of Physics Part 2', (Boston, MA, USA: Addison-Wesley Publishing Company Inc., 1964).
[3] L. D. Landau and E. M. Lifschitz, in 'Lehrbuch der theoretischen Physik, Bd. VIII: Elektrodynamik der Kontinua' [engl.: Textbook of Theoretical Physics, vol. VIII: Electrodynamics of Continuous Media], (Akademie-Verlag, Berlin, 1985).
[4] O. Stenzel and A. Macleod, Adv. Opt. Technol. 1, 463–481 (2012).
[5] O. Stenzel, S. Wilbrandt, S. Yulin, N. Kaiser, M. Held, et al., Opt. Mater. Exp. 1, 278–292 (2011).
[6] F. Jenkner, Präparation von TiO_2-, ZrO_2- und HfO_2-Schichten mittels Elektronenstrahlverdampfen, Fachhochschule Jena/ Fraunhofer IOF, Bachelor thesis (2011).
[7] R. Schlegel, Untersuchung des Einflusses des Arbeitsgases auf die Eigenschaften von mittels PIAD hergestellten Tantalpentoxidschichten, Ernst-Abbe-Fachhochschule Jena, Fachbereich SciTec, Master thesis (2012).
[8] S. Pongratz and A. Zöller, J. Vac. Sci. Techn. A 10, 1897–1904 (1992).
[9] A. S. Ferlauto, G. M. Ferreira, J. M. Pearce, C. R. Wronski, R. W. Collins, et al., J. Appl. Phys. 92, 2424–2436 (2002).
[10] E. C. Freeman and W. Paul, Phys. Rev. B 20, 716–728 (1979).
[11] M. Landmann, T. Köhler, S. Köppen, E. Rauls, T. Frauenheim, et al., Phys. Rev. B 86, 064201-1–20 (2012).
[12] O. Stenzel, S. Wilbrandt, N. Kaiser, M. Vinnichenko, F. Munnik, et al., Thin Solid Films 517, 6058–6068 (2009).
[13] S. Jakobs, M. Lappschies, U. Schallenberg, O. Stenzel and S. Wilbrandt, Chin. Opt. Lett. 8, 73–77 (2010).
[14] D. Liu, Characterization of single layer oxide thin films prepared by PIAD and sputter deposition on different substrates, Report on practical studies, Fraunhofer IOF (2012).

[15] O. Stenzel, S. Wilbrandt, M. Schürmann, N. Kaiser, H. Ehlers, et al., Appl. Opt. 50, C69–C74 (2011).
[16] L. D. Landau and E. M. Lifschitz, in 'Quantenmechanik', (Akademie-Verlag, Berlin, 1967).
[17] O. Stenzel, J. Phys. D 42, 055312 (2009).
[18] I. W. Donald and P. W. McMillan, J. Mater. Sci. 13, 2301–2312 (1978).
[19] R. W. Tustison, SPIE Proc. CR39, 231–240 (1992).
[20] J. H. Dobrowolski, F. C. Ho and A. Waldorf, Appl. Opt. 22, 3191–3196 (1983).
[21] O. Stenzel, S. Wilbrandt, K. Friedrich and N. Kaiser, Vak. Forsch. Prax. 21(5), 15–23 (2009).
[22] J. A. Woollam, B. Johs, C. Herzinger, J. Hilfiker, R. Synowicki, et al., SPIE Proc. CR72, 3–28 (1999).
[23] S. Wilbrandt, O. Stenzel and N. Kaiser, Proc. SPIE 7101, [71010D-1]–[71010D-11] (2008).
[24] O. Stenzel, M. Schürmann, S. Wilbrandt, N. Kaiser, A. Tünnermann, et al., Proc. SPIE 8168 81681W-1–81681W-10 (2011).
[25] L. G. Parratt, Phys. Rev. 95, 359–369 (1954).

Olaf Stenzel finished his diploma thesis in laser spectroscopy at the physics department of Moscow State University, Russia, in 1986. He received his PhD from Chemnitz University of Technology, Germany, in 1990 and habilitated there in 1999 in the field of optical properties of heterogeneous optical coatings. From 2001, he has worked at the Optical Coating Department of Fraunhofer Institute for Applied Optics and Precision Engineering IOF in Jena, Germany. He is the author of *The Physics of Thin Film Optical Spectra: An Introduction*, (Springer 2005).